Chapter 24

Basic Theory of RF Electron Linear Accelerator

– *J. Mondal*

Accelerator science plays a crucial role in the field of fundamental particle physics, industrial and medical applications. Acceleration of charge particles to required beam energy, current and size is possible both in circular and liner accelerators. This chapter emphisizes on the physics of radio frequency (RF) linear accelerator.

24.1 Introduction

Low energy electron accelerators have many societal applications as in food and agriculture section, industrial applications, radiotherapy machines for cancer treatment, radio isotope productions, waste water treatment etc. The schematic of a linear accelerator system is shown in Fig. 24.1. This short report presents the working principle of thermionic electron

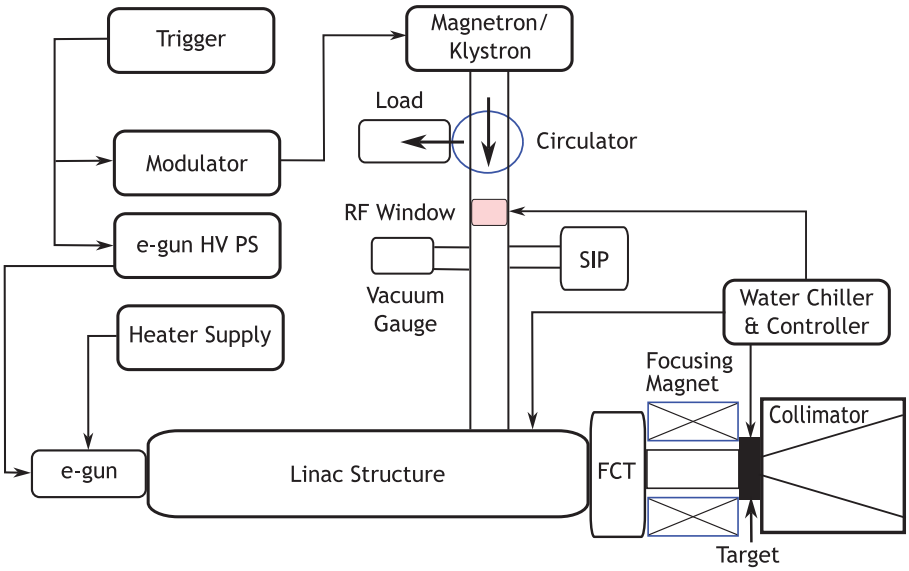

Figure 24.1: Schematic of a linear accelerator.

gun and RF Linac, single cell RF cavity, multicell RF cavity, different types of linac cavity structures, longitudinal and transverse beam dynamics in RF linac cavity.

24.2 RF Linear Accelerator

In a DC accelerator the maximum beam energy is limited by the discharge effects of the high voltage source. In RF Linear accelerator multiple gaps or cavities are arranged in proper phase relationship in order to provide incremental energy gain each cavity to reach final energy of the output beam. This section will describe the basic working principle of acceleration of charged particles in RF field, single cell RF cavity, multi-cell coupled cavity followed by different configurations of Linac.

24.2.1 Working Principles of RF Accelerator

In its simplest form the RF accelerator can be thought of a series of metallic drift tubes separated by a gap as shown in Fig. 24.2. The charged particles are accelerated by the electric fields in the gap between the drift tubes connected alternatively to the poles of an

AC generator. If the length of the tubes increases with the particle velocity during the acceleration such that the time of flight is kept constant and equal to half of the RF period, the particles are subject to a synchronous accelerating voltage and experience an energy gain of $\Delta W = q \times \Delta V$ at each gap crossing. The kinetic energy (KE) after the nth gap (K_n) is given by,

$$K_n = nqV_0 sin\psi_0 = \frac{1}{2}mv_n^2 \tag{24.1}$$

where ψ_0 is the phase of RF voltage seen by the particle and also the velocity after nth gap (v_n) is,

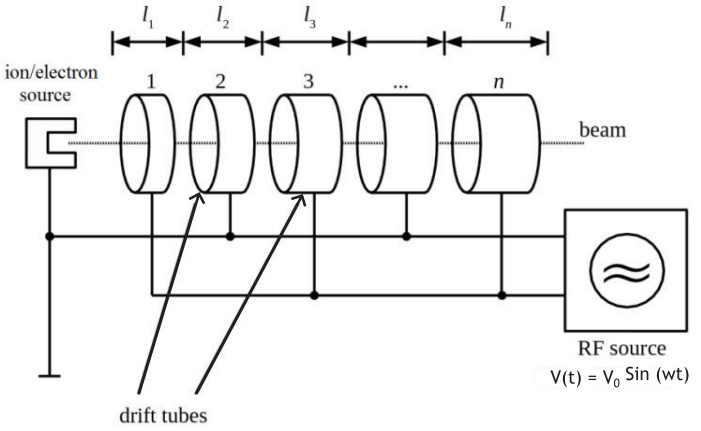

Figure 24.2: Schematic of RF acceleration in a series of gap-drift sections.

$$v_n = \sqrt{\frac{nqV_0 sin\psi_0}{m}} \tag{24.2}$$

In order to see the continuous accelerating field the time of travel from one gap to the other must be $T_{RF}/2$, where T_{RF} is the time period of RF field. Thus to maintain the travel time constant in subsequent gaps with increasing velocity, the length of drift tubes are increased. The length of nth drift tube (l_n) is,

$$l_n = v_n \frac{T_{RF}}{2} = \frac{1}{2}\beta_n \lambda_{RF} = \frac{\sqrt{n}}{f_{RF}} \sqrt{\frac{nqV_0 sin\psi_0}{m}} \propto \sqrt{n} \tag{24.3}$$

24.2.2 Pillbox Cavity

The gap and drift tube configuration are not suitable for high frequency RF structure because of large amount of radiative power loss. The high frequency electromagnetic waves are confined inside a high conductivity metal enclosure where the electric and magnetic fields oscillate in phase quadrature. Depending on the radius and boundary conditions there exist normal modes of resonances of different frequencies. Figure 24.3(a) shows the geometry of cylindrical pillbox cavity with radius R and length L. In order to accelerate electron beam we will consider only the transverse magnetic (TM_{010}) mode. The TM_{010} mode frequency,

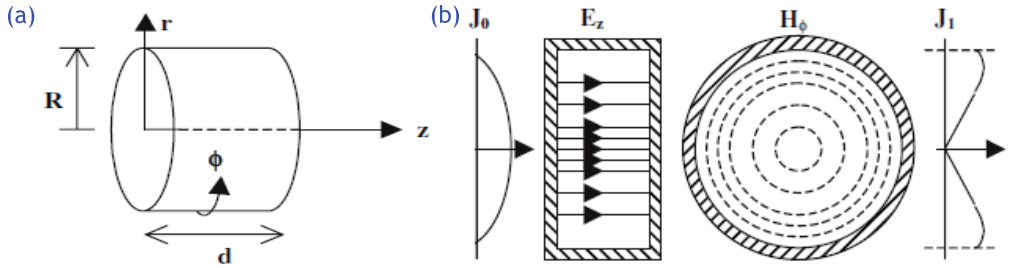

Figure 24.3: (a) Pillbox cavity, and (b) Electric and Magnetic fields in TM_{010} mode.

Electric and magnetic fields are given by,

$$f_0(GHz) = \frac{11.5}{R(cm)} \tag{24.4}$$

$$E_z = E_{0z} J_0(x_{01} r/R) exp(-j\omega_0 t) \tag{24.5}$$

$$H_\phi = j E_{0z} (\frac{\epsilon_0}{\mu_0})^{1/2} J_1(x_{01} r/R) exp(-j\omega_0 t) \tag{24.6}$$

The other field components are $E_r = E_\phi = H_r = H_z = 0$. Where E_{0z} = Maximum E-field at r = 0, J_0 and J_1 Bessel functions of zero and first orders, respectively, and ω_0 is the resonant frequency of TM_{010} mode. The total energy stored (U) in the cavity is calculated by integrating either the electric or magnetic energy density over the cavity volume. For the TM_{010} mode the total stored energy is given by,

$$U = \frac{\pi \epsilon_0}{2} E_{0z}^2 d R^2 J_1^2(2.405) \tag{24.7}$$

where $E_{0z} = \frac{\pi}{2} E_{acc}$. The average power loss is obtained by integrating the magnetic power density over the inner surface of the cavity. The average power loss in pill box cavity for the TM_{010} is given by,

$$P_c = \frac{\pi R_s E_{0z}^2}{\eta^2} J_1^2(2.405) R(d + R) \tag{24.8}$$

where, $R_s = \frac{\omega_0 \mu_0}{\sigma} (\Omega)$ and $e\eta = 377\ \Omega$. The quality factor Q_0 which is a measure of sharpness of cavity resonance and it is an important figure of merit and is defined as,

$$Q_0 = \frac{\omega_0 U}{P_c} = 1.73 \times 10^9 f_0^{-1/2} (1 + R/d)^{-1} \tag{24.9}$$

Another useful definition of cavity Q_0 is given by geometrical factor (G) and surface resistance R_s,

$$Q_0 = \frac{G}{R_s}; \text{where}, G = \frac{\omega_0 \mu_0 \iiint |\overrightarrow{H_\phi}|^2 dV}{\oint_S |\overrightarrow{H_\phi}|^2 dA} \tag{24.10}$$

Another important figure of merit is shunt impedance of the cavity. It actually shows the efficiency of acceleration through a cavity for a fixed energy gain. It is defined for TM_{010} mode as,

$$R_a = \frac{V_c^2}{P_c} = \frac{\pi \eta^2 d^2}{\pi^3 R_s J_1^2 R(R + d)} = 150 \left(\frac{d}{R}\right) Q_0 \tag{24.11}$$

24.2.3 Coupled Multi-cell Accelerating Cavity

First we will consider two pill box cavities joined together through a common beam pipe and an off axis slot as shown in Fig. 24.4a. The mechanical analogue of the two coupled cavity oscillator system is shown by two pendulums connected by a spring in Fig. 24.4b. When the pendulums are swinging in phase is called 0 mode. So in 0 mode the electric field is in the same direction for both the cavities meaning zero phase difference. When the pendulums are swinging in opposite directions is called π mode and cavity fields will be in opposite direction for π mode oscillations. It can be seen that for two coupled oscillators there exist only two normal modes. In analogy with this if N oscillators are coupled with a coupling constant k, it will have N such normal modes. The electrical equivalent circuit of

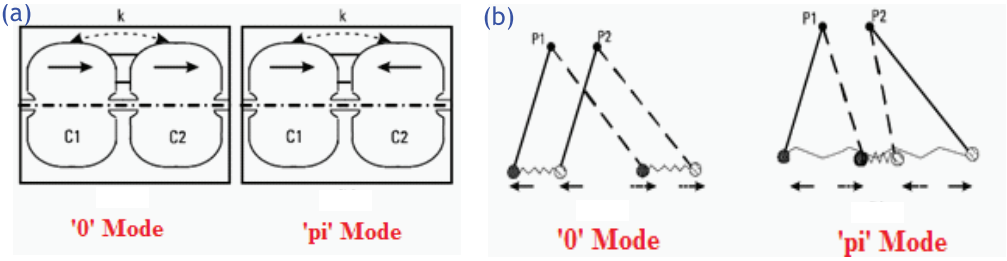

Figure 24.4: (a) Two coupled RF cavities, and (b) Two coupled pendulums.

coupled cavities is represented by a chain of resonant RLC circuits which are magnetically or capacitive coupled. To understand basic coupled cavity oscillators first we have considered three identical oscillators having uncoupled frequency f_r, coupling constant k and normalized field of amplitude of unity. It results in three normal modes. The frequencies and the normalized electric field of those modes are given in Table 24.1. The general case is a system consisting of (N+1) coupled oscillators. There are (N-1) identical internal oscillators terminated with half cells at each end. In this case, the normalized magnitudes of the eigenvectors i.e. electric fields of nth oscillator in mth mode are given by,

$$X_{mn} = \cos(\pi mn/N); \tag{24.12}$$

such that, n = 0, 1, ..., N (oscillator) and m = 0, 1, ..., N (mode), and the eigen frequency of mth mode is given by the following dispersion relationship,

$$\omega_m = \omega_r \left[1 + k\cos(\pi m/N)\right]^{-1/2}; k \approx (f_\pi - f_0)/f_{\pi/2} \tag{24.13}$$

The typical dispersion curve for seventeen cell coupled cavity is shown in Fig. 24.5. The pass band of the dispersion curve between the '0' mode and the π mode is decided by the coupling constant k. With the increase of cavity cells for a given coupling constant 'k', more and more normal modes are populated within the pass band and hence the normal mode frequencies become more closely spaced. It can be also seen that the $\pi/2$ mode is having the largest frequency separation between the next neighboring modes. Figure 24.6 shows a schematic of capacitive coupled cavity structure, where adjacent cavities are coupled by the electric field coupling through the beam aperture on the axis. Figure 24.7 shows the magnetic coupling scheme where adjacent cavities are coupled through a common slot in the high magnetic field region. The on axial electric field along the beam aperture exerts acceleration force on the charged particle beam. With the introduction of nose cone as shown in Fig. 24.8 at the iris region of each accelerating cell causes enhanced electric field density in axial direction and hence results in efficient acceleration. Accelerating structures become more efficient with increased shunt impedance. This can be achieved easily by reducing the beam aperture size.

Table 24.1: Frequency and electric field distribution of three coupled cavity.

Mode	Frequency	Normalized Electric field
0	$f_0 = f_r/\sqrt{1+k}$	$\begin{bmatrix}1\\1\\1\end{bmatrix}$
$\pi/2$	$f_{\pi/2} = f_r$	$\begin{bmatrix}1\\0\\-1\end{bmatrix}$
π	$f_0 = f_r/\sqrt{1-k}$	$\begin{bmatrix}1\\-1\\1\end{bmatrix}$

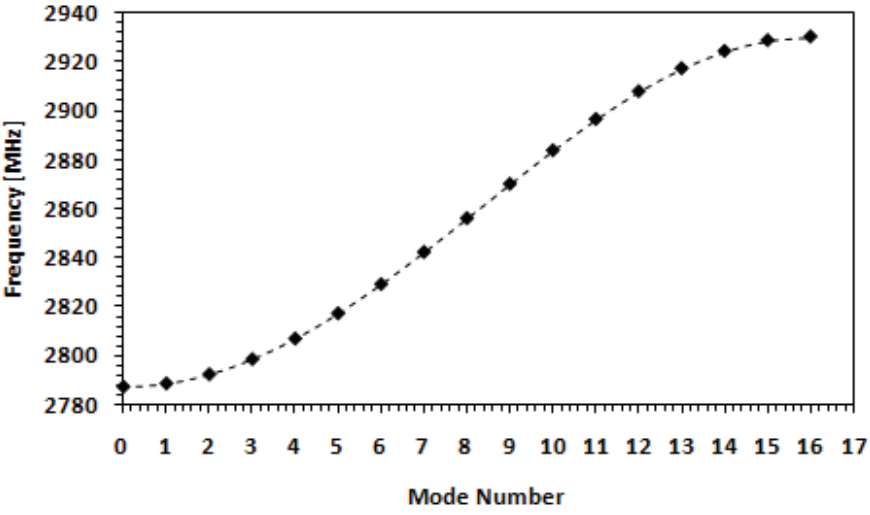

Figure 24.5: Dispersion relation of 17 coupled oscillators with k = 0.05, $f_{\pi/2}$ = 2856 MHz.

With reduced bore size the electric coupling becomes very negligible and hence a magnetic coupling is provided as shown in Fig. 24.7.

24.2.4 Different Configurations of RF Linear Accelerator

Low energy RF electron linear accelerators in the range of 1-15 MeV are being extensively used for industrial and medical applications. There are two types of RF accelerating structures namely standing-wave (SW) linac and the traveling-wave (TW) linac.

A. Standing wave Linac

As explained previously in case of SW linac structure, many individual cells are coupled together to form a cavity chain. The cavity chain is shorted at both ends. The RF power is fed though a cavity cell in the chain to establish required electric field in the SW linac structure. The basic schematic of SW linac is shown in Fig, 24.9. In SW structure the electric field builds up in time. Under pulsed operation the field build up is given by,

$$E(t) = E_{0z}\left[1 - exp(-\omega t/Q_L)\right]; Q_0 = (1+\beta)Q_L; \beta = Q_0/Q_{ext}. \tag{24.14}$$

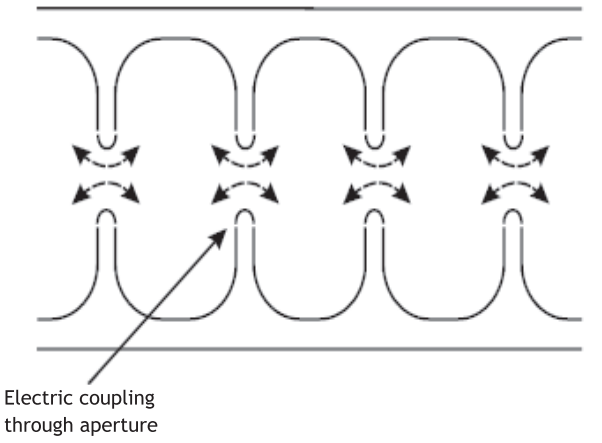

Figure 24.6: Electric coupling between cavities.

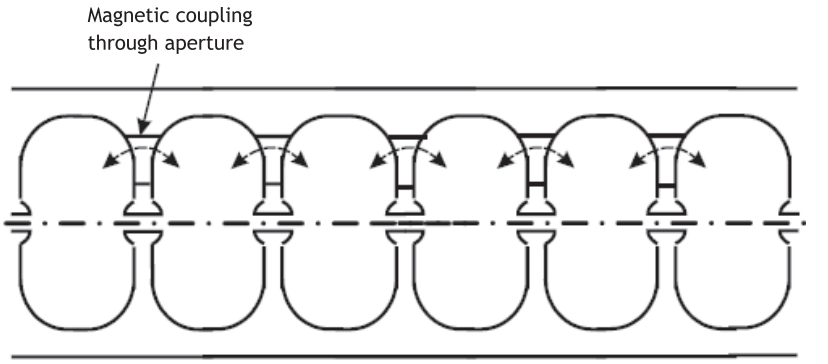

Figure 24.7: Magnetic coupling between cavities.

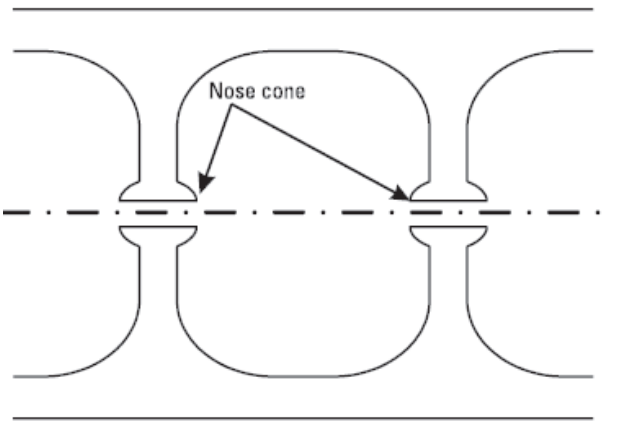

Figure 24.8: Introducing nose cones to enhance acceleration efficiency.

SW structures are generally operated in π and $\pi/2$ modes because of high shunt impedance

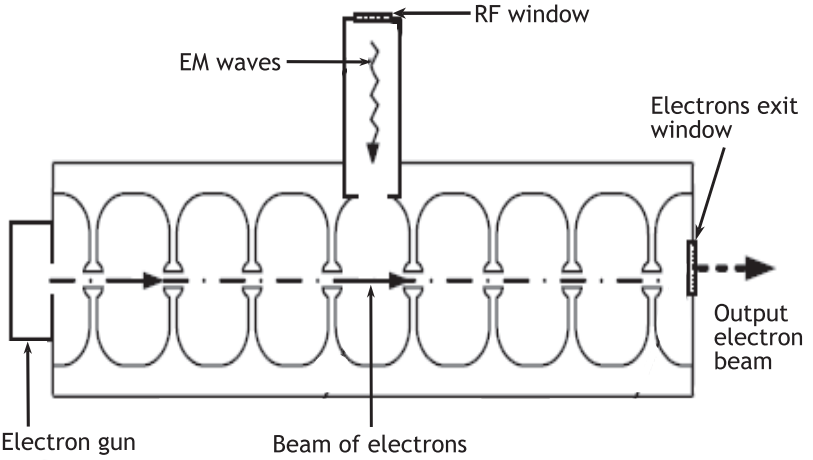

Figure 24.9: Basic Schematic of standing wave linac.

for these two modes. When number of coupled cavities are not large then π mode is preferred as separation of nearest neighbor frequency is large. Hence for large number of cells $\pi/2$ mode is chosen because of highest frequency separation with the nearest neighbors. But in case of a $\pi/2$ mode every alternate cell is unexcited and do not play any role in accelerating the beam as shown in Fig. 24.10(A). Hence in principle it is non efficient. But to overcome this a bi-

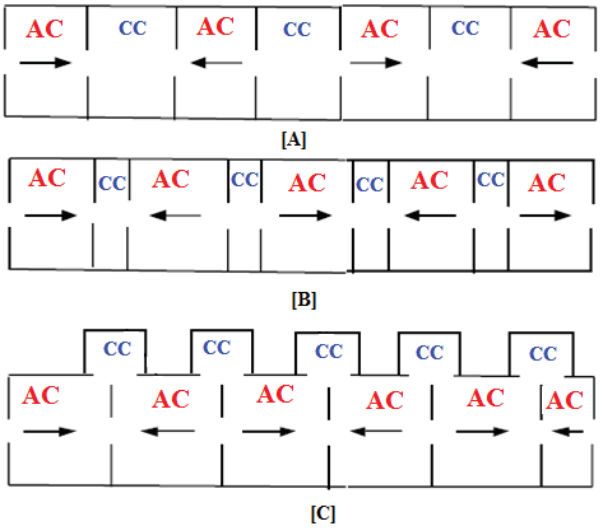

Figure 24.10: Different configurations of SW linac in $\pi/2$ mode.

periodic structure geometry is adopted. The first periodic chain consists of accelerating cells which are optimized with respect to highest shunt impedance and second chain is of coupling cells in between the accelerating cells are tuned to accelerating cell resonant frequency by reducing their axial dimensions (on axis) or shifting the coupling cell from the axis (off axis). The two most popular geometry are the on-axis and the off axis coupled bi-periodic

structure is shown in Fig. 24.10(B) and 24.10(C). The dispersion relation of a bi-periodic cavity structure is given by,

$$k_{ac}^2 \cos^2\phi = \left(1 - \frac{f_a^2}{f^2} + k_{aa} cos2\phi\right)\left(1 - \frac{f_c^2}{f^2} + k_{cc} cos2\phi\right) \tag{24.15}$$

where f is the resonance frequency of the coupled cavities at the ϕ mode, f_a and f_c are the resonance frequencies of the accelerating cavity and the coupling cavity, respectively and k_{ac} is the coupling coefficient between the accelerating cavity to the nearest coupling cavity, while that of k_{aa} for two neighbouring accelerating cavities and k_{cc} for two neighbouring coupling cavities; the stop band (SB) is defined as, $SB = \left| \frac{f_a}{\sqrt{1-k_{aa}}} - \frac{f_c}{\sqrt{1-k_{cc}}} \right|$. The design goal is to eliminate the stop band and make k_{aa} and k_{cc} to be nearly zero.

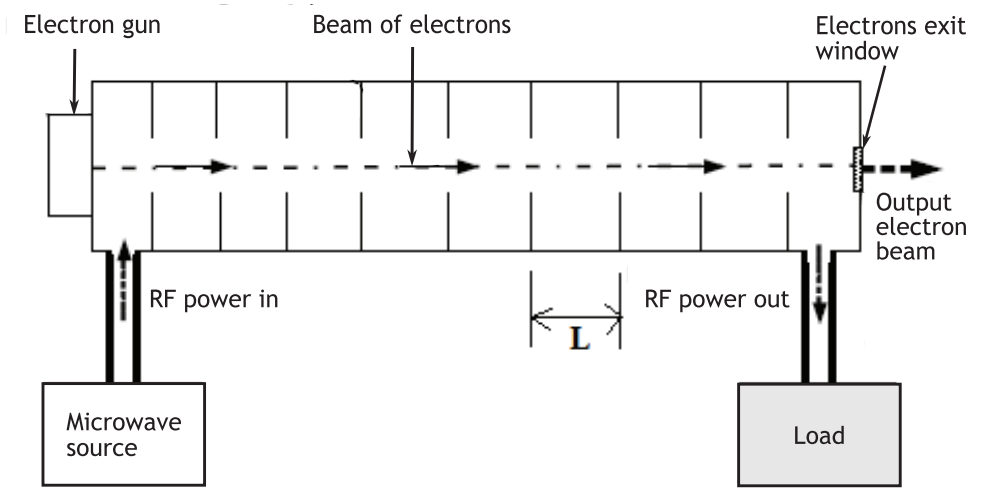

Figure 24.11: Disk-Loaded travelling wave structure.

B. Travelling wave Linac

In travelling wave linac structure microwave enters at the e-gun side and propagates through the structure and finally absorbed in a matched resistive load at the end of the structure. The schematic of the structure is shown in Fig. 24.11. The phase velocity of the TM_{010} mode in smooth walled waveguide is always higher than the speed of light and hence particle acceleration is not possible. In order to reduce the phase velocity of TM_{010} wave, disks are inserted with certain periodicity. This specific geometry is called as disk-loaded travelling wave cavity structure. The dispersion relation and phase velocity of a disk-loaded TW structure is given by,

$$\frac{\omega^2}{c^2} = K_r^2 + K_n^2; K_r = 2.405/a; K_n = k_0 + \frac{2\pi n}{L}; \text{and, } v_{ph} = \frac{\omega}{k_0 + \frac{2\pi n}{L}} < c \tag{24.16}$$

Travelling wave structures are two types namely constant impedance (CI) and constant gradient (CG). Figure 24.12 shows the schematic of CI and CG structures. In CI structure all cells are identical and hence electric field amplitude is continuously decreases as the wave travels towards the load end. Where as in CG structure by tapering the beam aperture the group velocity is varied and hence the electric field gradient throughout the structure remains constant.

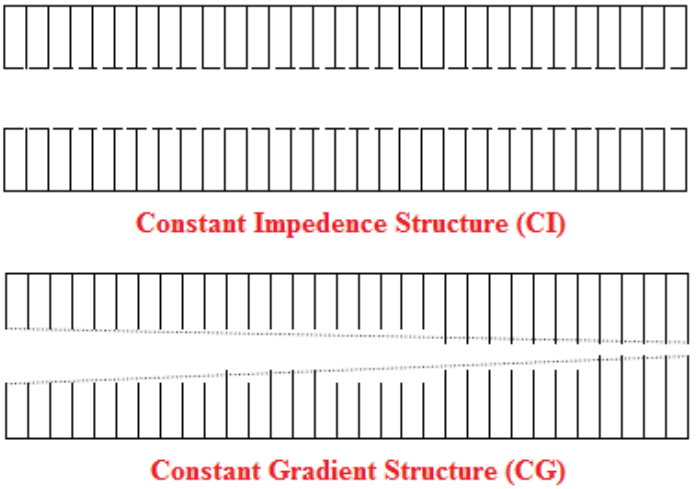

Figure 24.12: CI and CG travelling wave structure.

24.3 Fundamentals of Beam Dynamics in RF Accelerator

24.3.1 Longitudinal Beam Dynamics

The fundamental equations of beam dynamics in RF linac for low current beam are given by,

$$\frac{d\gamma}{dz} = \left(\frac{-eE_{0z}}{mc^2}\right)\sin\theta; \tag{24.17}$$

$$\frac{d\theta}{dz} = \left(\frac{2\pi}{\lambda}\right)\left(\frac{1}{\beta_s} - \frac{1}{\beta}\right) \tag{24.18}$$

Here, $\gamma = 1/\sqrt{1-\beta_e^2}$, β_s = Synchronous particle velocity, β_e = velocity of the other particle, θ = Phase of the other particle with respect to synchronous particle, λ = free space wavelength. Solving these equations introducing the reduced momentum $p = \beta\gamma$,

$$\cos\theta - \cos\theta_m = \frac{2\pi mc^2}{eE_{0z}\lambda}\left(\sqrt{1+p^2} - \sqrt{1-\beta_s^2} - \beta_s p\right) \tag{24.19}$$

The phase extrema $\theta = \pm\theta_m$ occurs when $\beta_e = \beta_s$ with trajectories in longitudinal phase space plotted in Figs. 24.13 (a) &(b) for the two cases, $\beta_s < 1$ and $\beta_s = 1$, respectively. The orbits are parameterized by $\pm\theta_m$, the limits of the θ excursion occurring for $\beta = \beta_s$. For the $\beta_s = 1$ case, θ_∞ denotes the asymptotic phase which an electron approaches as p tends to infinity. For $\beta_s = 1$ the orbit equation is simpler,

$$\cos\theta - \cos\theta_m = \frac{2\pi mc^2}{eE_{0z}\lambda}\left(\sqrt{1+p^2} - p\right) \tag{24.20}$$

In practice, θ_∞ = -π/2 is the ideal for acceleration at the peak of the wave. With the beam entering the structure near $\theta = 0$, an operating field corresponding to the input,

$$E_{0z} = \frac{2\pi mc^2}{e\lambda}\left(\sqrt{1+p_0^2} - p_0\right) \tag{24.21}$$

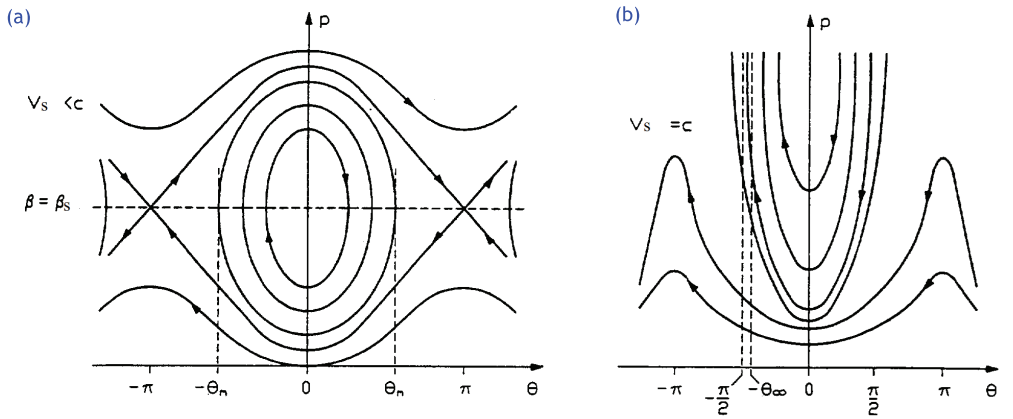

Figure 24.13: (a) Phase space orbits for $\beta_s < 1$, and (b) Phase space orbits for $\beta_s = 1$.

24.3.2 Transverse Beam Dynamics

The RF field in a cavity structure exerts radial forces on off axis particles along with the acceleration forces. As shown in Fig. 24.14(a) off axis particle at the entrance of RF cavity sees a focusing force whereas the Fig. 24.14(b) shows that at the exit it will see defocusing force. The net effect is decided by three counter effects namely the variation of electric fields with time, radial displacement of particle at the entrance and exit and change in particle velocity along the acceleration gap.

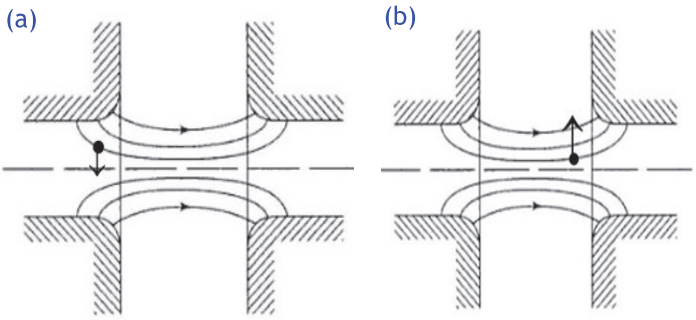

Figure 24.14: (a) Focusing force at the entrance, and (b) Defocusing force at the exit.

A. Radial Electric and Azimuthal Magnetic Field Near the Axis of TM_{010} Mode

In case of TM_{010} mode only non zero components of the fields are E_z, E_r and B_θ. The Maxwell's equations for non zero components of the field are,

$$\frac{1}{r}\frac{\partial(rE_r)}{\partial r} + \frac{\partial E_z}{\partial z} = 0; \text{from}, \nabla.\vec{E} = 0 \tag{24.22}$$

$$\frac{\partial E_r}{\partial r} - \frac{\partial E_z}{\partial z} = -\frac{\partial B_\theta}{\partial t}; \text{from}, \left(\nabla \times \vec{E}\right)_\theta = -\frac{\partial B_\theta}{\partial t} \tag{24.23}$$

$$-\frac{\partial B_\theta}{\partial z} = -\frac{1}{c^2}\frac{\partial E_r}{\partial t}; \text{from}, \left(\nabla \times \vec{B}\right)_r = \frac{1}{c^2}\frac{\partial E_r}{\partial t} \tag{24.24}$$

$$\frac{1}{r}\frac{\partial(rB_\theta)}{\partial r} = \frac{1}{c^2}\frac{\partial E_z}{\partial t}; \text{from}, \left(\nabla \times \vec{B}\right)_z = \frac{1}{c^2}\frac{\partial E_z}{\partial t} \tag{24.25}$$

Near the axis we can approximate that E_z is not dependent on r. With this assumption Eq. (24.25) can be rewritten as,

$$rE_r = -\frac{\partial E_z}{\partial z}\int_0^r r dr; \text{then}, E_r = -\frac{1}{2}\frac{\partial E_z}{\partial z}, \text{and then}, \frac{\partial E_r}{\partial r} = -\frac{1}{2}\frac{\partial E_z}{\partial z} \tag{24.26}$$

Similarly from Eq. (24.26) we get,

$$B_\theta = -\frac{r}{2c^2}\frac{\partial E_z}{\partial t}, \text{and}, \frac{\partial B_\theta}{\partial r} = -\frac{1}{2c^2}\frac{\partial E_z}{\partial t} \tag{24.27}$$

B. Transverse Impulse in Standing Wave Linac Gap

In a standing wave linac the z component of electric field varies with position as well as time. It can be written as,

$$\frac{dE_z}{dz} = \frac{\partial E_z}{\partial z} + \frac{1}{\beta c}\frac{\partial E_z}{\partial t}, \text{where}, E_z(z) = E_0 J_0(K_r r)\cos(\omega t + \phi) \tag{24.28}$$

The change in radial momentum is derived from Lorentz force equation,

$$F_r = qE_r + q\beta c B_\theta \tag{24.29}$$

Inserting values of E_r and B_θ from Eq. (24.26) and Eq. (24.27) into Eq. (24.29) will give the change in radial momentum,

$$\Delta p_r = \frac{qr}{2\beta c}\int_{-L/2}^{L/2}\left[\frac{dE_z}{dz} - \left(\frac{\beta}{c} - \frac{1}{\beta c}\right)\frac{\partial E_z}{\partial t}\right]dz \tag{24.30}$$

Inserting E_z(z) from Eq. (24.28) into Eq. (24.30) and doing some simple steps of mathematics it will result in normalized change in radial momentum,

$$\Delta(\gamma\beta r') = \frac{\pi q E_0 T L \sin\phi}{mc^2\gamma^2\beta^2 L} r \tag{24.31}$$

where, $T = \frac{\sin(\pi L/\lambda)}{(\pi L/\lambda)}$.

24.4 Conclusions

This chapter discusses the basic theory of RF linac cavity design. It also discusses the preliminary equations which governs the beam dynamics in the cavity structure.

Suggestions for Further Reading

a) [123–126]